Selective bond formation triggered by short optical pulses: Quantum dynamics of a four-center ring closure

Alessio Valentini[1], Stephan van den Wildenberg[1], and F. Remacle[1*]

1. Theoretical Physical Chemistry, MOLSYS Research Unit, University of Liège, Liège, Belgium

Electronic Supplementary Information

Content

Table S3: Cartesian coordinates of the displacement vector of the unfrozen atoms for the φ coordinate.

Table S4: Vertical excitation energies of the electronic states of norbornadiene

Table S5: Transition dipole moment of norbornadiene at the equilibrium geometry

Table S6: Transition dipoles at the geometry of the minimum energy of the S_0/S_1 conical intersection.

S1. Definition of the three coordinates used to define the grid for quantum dynamics

The 3-dimensional grid used to describe the isomerization process of norbornadiene to quadricyclane is defined as follows. The equilibrium geometries of the norbornadiene and quadricyclane isomers on the ground state were determined at the SA(14)-CASSCF(4,8)/AUG-cc-pVDZ level of theory; see Tables S1 and S2 for the cartesian coordinates and section S2 for the details on the electronic structure computations. Since the coordinates of the C_3H_4 bridge (atoms C1, C2, C3, H4, H5, H6 and H7 in Figure S1A) do not vary significantly in the two isomers, they were frozen at their values in the equilibrium geometry of the GS of norbornadiene to define the 3D grid, see Figure S1 A, B, C for the labeling of the atoms and Table S1 for the values.

The motions of the atoms of the C_4H_4 ring are described using a system of three coordinates. As discussed in the main text, we define two angles, θ and γ which describe the ring closure. These angles can be qualitatively related to two normal modes of both norbornadiene and quadricyclane. The angle θ corresponds to the symmetric bending mode that modifies the C11-C10 and C8-C9 distances ('new' bonds formed in quadricyclane) and γ to the symmetric stretching C11-C8 and C10-C9 distances ('old' π bonds that are present in norbornadiene). The third coordinate, φ, parametrizes the distortion of the geometry at the minimum of the S_0/S_1 conical intersection (CI), see Figure S3.

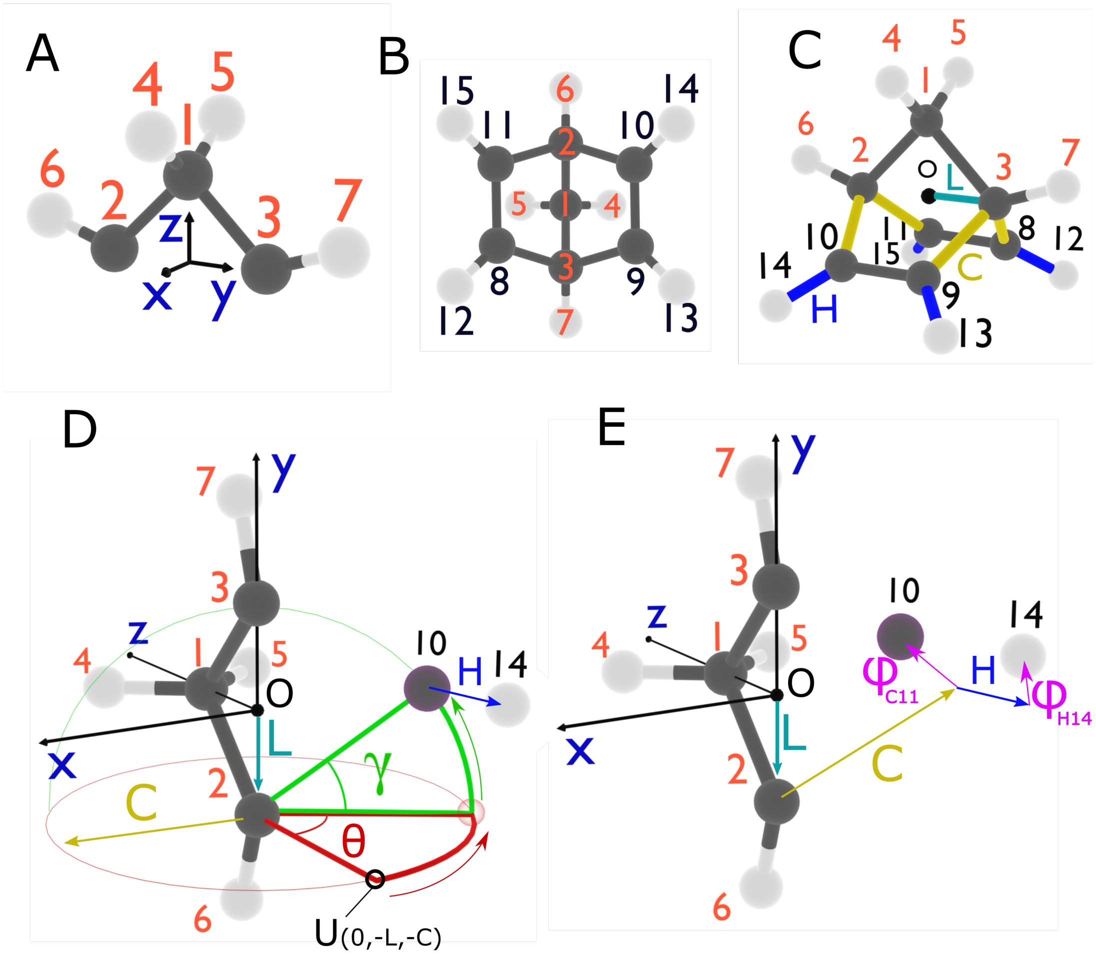

Figure S1. Reduced set of three coordinates A) The 7 frozen atoms, C1, C2, C3, H4, H5, H6 and H7, of the C_3H_4 bridge and the Cartesian frame. B) Atom labels: the frozen atoms of the bridge are labeled in orange and the atoms of the C_4H_4 ring (C8,C9,C10,C11, H12,H13,H14,H15) whose motions are described by the coordinates θ,γ,φ in black. C) The three lengths, L, C and H, that are kept constant in defining the coordinates θ,γ,φ. L is the distance between the origin of the Cartesian frame and the atoms C2 or C3, C is the length of the four bonds: C2-C10, C2-C11, C3-C8 and C3-C9. H is the length of the four C-H bonds of the ring : C10-H14, C9-H13, C8-H12 and C11-H15. The values of L, C and H are fixed at their values at the norbornadiene equilibrium geometry. D) Definition of the Cartesian coordinates of the atoms C10 and H14 in terms of the coordinates θ,γ. When θ and γ are equal to zero, the C10 Cartesian coordinates are at point U with coordinates (0,-L,-C). The H14 coordinates are obtained by adding the same displacement from the atom C10 as in the norbornadiene equilibrium geometry. E) The φ coordinate corresponds to a linear displacement applied to the Cartesian coordinates of the H and C atoms of the ring that are defined by the values of the θ and γ. The expressions of the Cartesian coordinates of the 8 atoms of the C_4H_4 ring in terms of the coordinates θ, γ and φ are given in Eqs. S2 and S3 below.

The cartesian frame orientation is shown in Figure S1A. The y axis passes through the C2 and C3 atoms of the frozen bridge, with its origin in the middle of the C2-C3 distance. This distance is a constant that we constrain to be equal to 2L, with L = 1.116Å since the bridge is frozen. The z axis contains the C1 atom of the bridge. The atoms C1, C2, C3 and H6 and H7 are in the (z,y) plane. The coordinates of the frozen atoms of the bridge in this cartesian frame correspond to the first 7 atoms of Table S1.

Table S1. Cartesian coordinates of the atoms at the equilibrium geometry of norbornadiene in Å computed at the SA(14)-CASSCF(4,8)/AUG-cc-pVDZ. The first 7 atoms are the atoms of the frozen C_3H_4 bridge.

atom	x	y	z
C1	0.000	0.000	1.078
C2	0.000	-1.116	0.000
C3	0.000	1.116	0.000
H4	0.895	0.000	1.699
H5	-0.895	0.000	1.699
H6	0.000	-2.149	0.337
H7	0.000	2.149	0.337
C8	-1.240	0.662	-0.794
C9	1.240	0.662	-0.794
C10	1.240	-0.662	-0.794
C11	-1.240	-0.662	-0.794

H12	-1.935	1.324	-1.288
H13	1.935	1.324	-1.288
H14	1.935	-1.324	-1.288
H15	-1.935	-1.324	-1.288

Two other groups of 4 distances equal by symmetry in the equilibrium geometry of the norbornadiene GS are kept fixed in order to define the θ,γ,φ coordinates: the four C3-C8, C3-C9, C2-C10 and C2-C11 distances, labeled C in Figure S1C, are fixed to 1.541 Å and the four C8-H12, C9-H13, C10-H14 and C11-H15 distances, labeled H in Figure S1C are fixed to 1.077 Å. These distances do not differ much from the quadricyclane equilibrium geometry ones, see Tables S1 and S2.

Table S2: Cartesian coordinates of the atoms at the equilibrium geometry of quadricyclane in Å computed as the SA(14)-CASSCF(4,8)/AUG-cc-pVDZ.

atom	x	y	z
C1	0.000	0.000	1.078
C2	0.000	-1.116	0.000
C3	0.000	1.116	0.000
H4	0.895	0.000	1.699
H5	-0.895	0.000	1.699
H6	0.000	-2.149	0.337
H7	0.000	2.149	0.337
C8	-0.785	0.733	-1.270
C9	0.785	0.733	-1.270
C10	0.785	-0.733	-1.270
C11	-0.785	-0.733	-1.270
H12	-1.480	1.395	-1.764
H13	1.480	1.395	-1.764
H14	1.480	-1.395	-1.764
H15	-1.480	-1.395	-1.764

The three coordinates, θ,γ,φ are defined in the Cartesian frame as shown in Figure S1D-S1E for the atoms C10 and H14. Technically, the θ and γ are defined as rotations and φ parametrizes a displacement vector.

As shown in Figure S1D for C10, since the distance C is constant, θ is the angle between the projection of the position vector of C10 in the (x, z) plane translated by -L along y to the C2 atom of the bridge and the z axis. When θ =0 C10 is in the (z, y) plane. A positive θ value corresponds to clockwise rotation of C9 and C11 in the (x,z) plane and to counterclockwise one of C8 and C10. For C10, γ is the angle between the position vector of the atom and its projection in the (x, z) plane translated by -L along y to the C2 atom of the bridge. As the positions of the carbon atoms C2 and C3 of the bridge are kept fixed along the y axis, it is helpful to visualize the γ angle as a complementary angle of C3-C2-C10.

φ parametrizes a linear displacement vector defined to reach distorted geometries close to the geometry of the minimum energy S_1/S_0 conical intersection determined by keeping the coordinates of the C_3H_4 frozen as explained above. The Cartesian components of the displacement vector are added to the Cartesian components of the atoms of the C_4H_4 ring at the geometry defined by the values of θ and φ as shown in Figure S1E. It is defined by the following transformations:

- The geometry corresponding to the minimum energy conical intersection S_1/S_0 is determined by relaxing the coordinates of the unfrozen atoms only. This geometry is labeled D_A.
- The closest geometry to D_A is generated on the 2dimensional grid using the coordinates θ and γ. This geometry is labeled D_B.
- The displacement vector $\mathbf{D} = \mathbf{D}_B - \mathbf{D}_A$ is calculated by subtracting the Cartesian coordinates of the atoms at the geometry D_A from the ones of D_B. The first 7x 3 Cartesian components of **D** are 0 since they correspond to the atoms of the frozen bridge. The Cartesian coordinates of the displacement vector **D** of the 8 atoms of the ring are given in Table S3.

Table S3: Cartesian coordinates of the displacement vector **D** in Å for the 8 atoms of the ring

atom	x	y	z
C8	-0.166	0.067	0.016
C9	-0.145	-0.096	-0.144
C10	0.165	-0.068	0.016
C11	0.146	0.096	0.144
H12	0.521	0.086	0.317
H13	0.450	0.048	0.245
H14	0.520	0.087	0.317
H15	0.452	0.047	0.246

The displacement D_f corresponding to a value of φ is defined as:

$$\mathbf{D}_f = \frac{\varphi}{\varphi_{CI}} \mathbf{D} \qquad \text{(S1)}$$

The constant φ_{CI} is chosen to be -0.06 so that the three coordinates (θ, γ, φ) are commensurable with each other, for the stability of the numerical integration. When $\varphi = \varphi_{CI}$, the displacement $\mathbf{D_f}$ is equal to **D** and the conical intersection geometry $\mathbf{D}_A$ is then spanned by the 3D grid.

In terms of the three coordinates (θ, γ, φ) and of the frozen distances L and C, the Cartesian coordinates of the 4 unfrozen C atoms of the C_4H_4 ring take the form:

$$
\begin{aligned}
C8_x &= -Csin(\theta)cos(\gamma) + \frac{\varphi}{\varphi_{CI}} D_x^{C8} & \qquad C9_x &= -Csin(-\theta)cos(\gamma) + \frac{\varphi}{\varphi_{CI}} D_x^{C9} \\
C8_y &= L - Csin(\gamma) + \frac{\varphi}{\varphi_{CI}} D_y^{C8} & \qquad C9_y &= L - Csin(\gamma) + \frac{\varphi}{\varphi_{CI}} D_y^{C9} \\
C8_z &= -Ccos(\theta)cos(\gamma) + \frac{\varphi}{\varphi_{CI}} D_z^{C8} & \qquad C9_z &= -Ccos(-\theta)cos(\gamma) + \frac{\varphi}{\varphi_{CI}} D_z^{C9} \\
\\
C10_x &= Csin(\theta)cos(\gamma) + \frac{\varphi}{\varphi_{CI}} D_x^{C10} & \qquad C11_x &= Csin(-\theta)cos(\gamma) + \frac{\varphi}{\varphi_{CI}} D_x^{C11} \\
C10_y &= -L + Csin(\gamma) + \frac{\varphi}{\varphi_{CI}} D_y^{C10} & \qquad C11_y &= -L + Csin(\gamma) + \frac{\varphi}{\varphi_{CI}} D_y^{C11} \\
C10_z &= -Ccos(\theta)cos(\gamma) + \frac{\varphi}{\varphi_{CI}} D_z^{C10} & \qquad C11_z &= -Ccos(-\theta)cos(\gamma) + \frac{\varphi}{\varphi_{CI}} D_z^{C11}
\end{aligned}
\tag{S2}
$$

Since the four C8-H12, C9-H13, C10-H14 and C11-H15 distances are kept frozen to the value H, for $\varphi = 0$, the cartesian coordinates of the hydrogen atoms are obtained by adding a fixed displacement to the coordinates of the carbon atoms: $x_H = +0.695$ Å, $y_H = +0.661$ Å, $z_H = +0.494$ Å. They are then modified by the displacement vector that corresponds to the φ coordinate.

$$\begin{aligned}
H12_x &= -Csin(\theta)cos(\gamma) + \frac{\varphi}{\varphi_{CI}} D_x^{H12} - x_H & \quad H13_x &= -Csin(-\theta)cos(\gamma) + \frac{\varphi}{\varphi_{CI}} D_x^{H13} + x_H \\
H12_y &= L - Csin(\gamma) + \frac{\varphi}{\varphi_{CI}} D_y^{H12} + y_H & \quad H13_y &= L - Csin(\gamma) + \frac{\varphi}{\varphi_{CI}} D_y^{H13} + y_H \\
H12_z &= -Ccos(\theta)cos(\gamma) + \frac{\varphi}{\varphi_{CI}} D_z^{H12} - z_H & \quad H13_z &= -Ccos(-\theta)cos(\gamma) + \frac{\varphi}{\varphi_{CI}} D_z^{H13} - z_H
\end{aligned}$$

$$\begin{aligned}
H14_x &= Csin(\theta)cos(\gamma) + \frac{\varphi}{\varphi_{CI}} D_x^{H14} + x_H & \quad H15_x &= Csin(-\theta)cos(\gamma) + \frac{\varphi}{\varphi_{CI}} D_x^{H15} - x_H \\
H14_y &= -L + Csin(\gamma) + \frac{\varphi}{\varphi_{CI}} D_y^{H14} - y_H & \quad H15_y &= -L + Csin(\gamma) + \frac{\varphi}{\varphi_{CI}} D_y^{H15} - y_H \\
H14_z &= -Ccos(\theta)cos(\gamma) + \frac{\varphi}{\varphi_{CI}} D_z^{H14} - z_H & \quad H15_z &= -Ccos(-\theta)cos(\gamma) + \frac{\varphi}{\varphi_{CI}} D_z^{H15} - z_H
\end{aligned}$$

(S3)

In total, 65000 points are included in the grid: 100 in θ, 26 in γ and 25 in φ. The range in each coordinate is [1.08:0.7] for θ, [0.21:0.34] for γ and [-0.070: 0.05] for φ. $d\theta$=-0.386, $d\gamma$ = 0.134, and $d\varphi$=0.12. γ and θ are given in radians and φ is dimensionless.

For each of the 65000 grid points, the electronic structure has been computed at the SA(14)-CASSCF(4,8)/AUG-cc-pVDZ level, see section 2, and the energies, transition dipoles and non adiabatic vectors stored.

The values of θ, γ and φ for the equilibrium geometries of norbornadiene, quadricyclane and the minimum energy S_0/S_1 conical intersection are (1.001, 0.299, 0.0) for norbornadiene, (0.553, 0.251, 0.0) for quadricyclane and (0.763, 0.208, -0.066) for the S_0/S_1 minimum energy along the conical intersection seam. In order to keep the number of grid points manageable from a computational resources point of view when running the quantum dynamics, the range of the θ coordinate does not allow to reach the quadricyclane equilibrium geometry in the grid.

The deformations induced by the displacement that corresponds to the three coordinates preserve a C2 symmetry of the nuclear frame for all the 65000 grid points. In the plane $\varphi = 0$, a C2v geometry of the nuclear frame is preserved. We show in figure S2 the atom displacements that correspond to θ, γ and φ respectively. As explained above, θ corresponds to a symmetric bending motion and belongs to the totally symmetric representation of the C2v group for the nuclear frame, as well as γ which corresponds to a symmetric stretching of the C8-C11 and C9-C10 bonds and belongs to A1 irreducible representation of C2v. The φ distortion belongs to the A irreducible representation of the C2 point group.

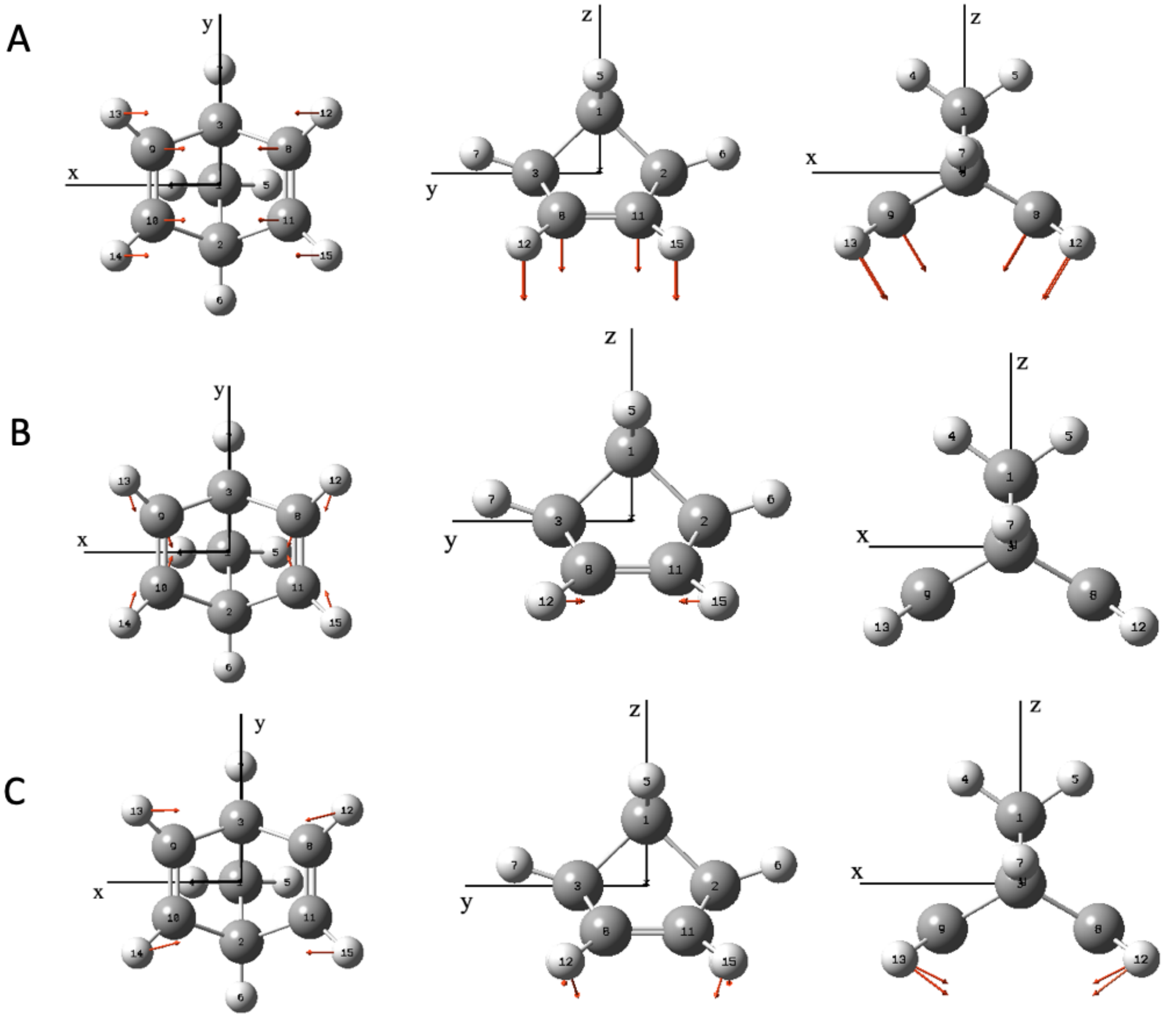

Figure S2. Atomic displacements corresponding to the three coordinates A) θ, B) γ and C) φ. Left, view in the (x,y) plane. Middle, view in the (y,z) plane. Right, view in the (x,z) plane. Note that in this view, the atoms H12 and H15 are perfectly in front of H13 and H14, making it seem like there are two arrows on H12 and H15. Right, view in the (x,z) plane. In this view, H13 and H12 superimpose H14 and H15, making it seem like there are two arrows on H13 and H12.

S2. Electronic structure

S2.1 Electronic states and transition dipoles

The electronic structure was computed using the OpenMOLCAS software, version 8.1[1]. The changes in the electronic structure that accompany the isomerization process involve valence and Rydberg excited states, which continuously exchange character. We therefore use the diffuse atomic basis set CC-PVDZ for the hydrogen atoms and AUG-CC-PVDZ for the carbon atoms in order to correctly describe Rydberg states. We determined that the level of theory SA(14)-CASSCF(4,8) is a good compromise to converge the electronic structure calculation for the 65000 geometries corresponding to the grid points and obtain the potential energies, transition dipole moments and nonadiabatic couplings vectors that are the inputs of the quantum dynamical computations. The active space has been chosen to consistently describe several excited states across the geometries spanned by our coordinates; 4 electrons, 23 inactive molecular orbitals (MO) and 8 active MO's are used. The set of active MO orbitals includes 4 valence bonding/antibonding MO's and 4 Rydberg MO's (see Figure S3). The choice of active MO's is based on a Walsh diagram analysis from the open form to the closed form using as reference the Hartree-Fock SCF orbitals. The equilibrium geometries of the norbornadiene and quadricyclane belong to the C_{2v} point group. Three active MO's belong to the A_1 irreducible representation, one to A_2, two to B_1 and two to B_2. We include 14 excited states in the state average procedure with equal weights in order to get a proper description of the lowest 7 excited states for all the geometries spanned by the 3D grid.

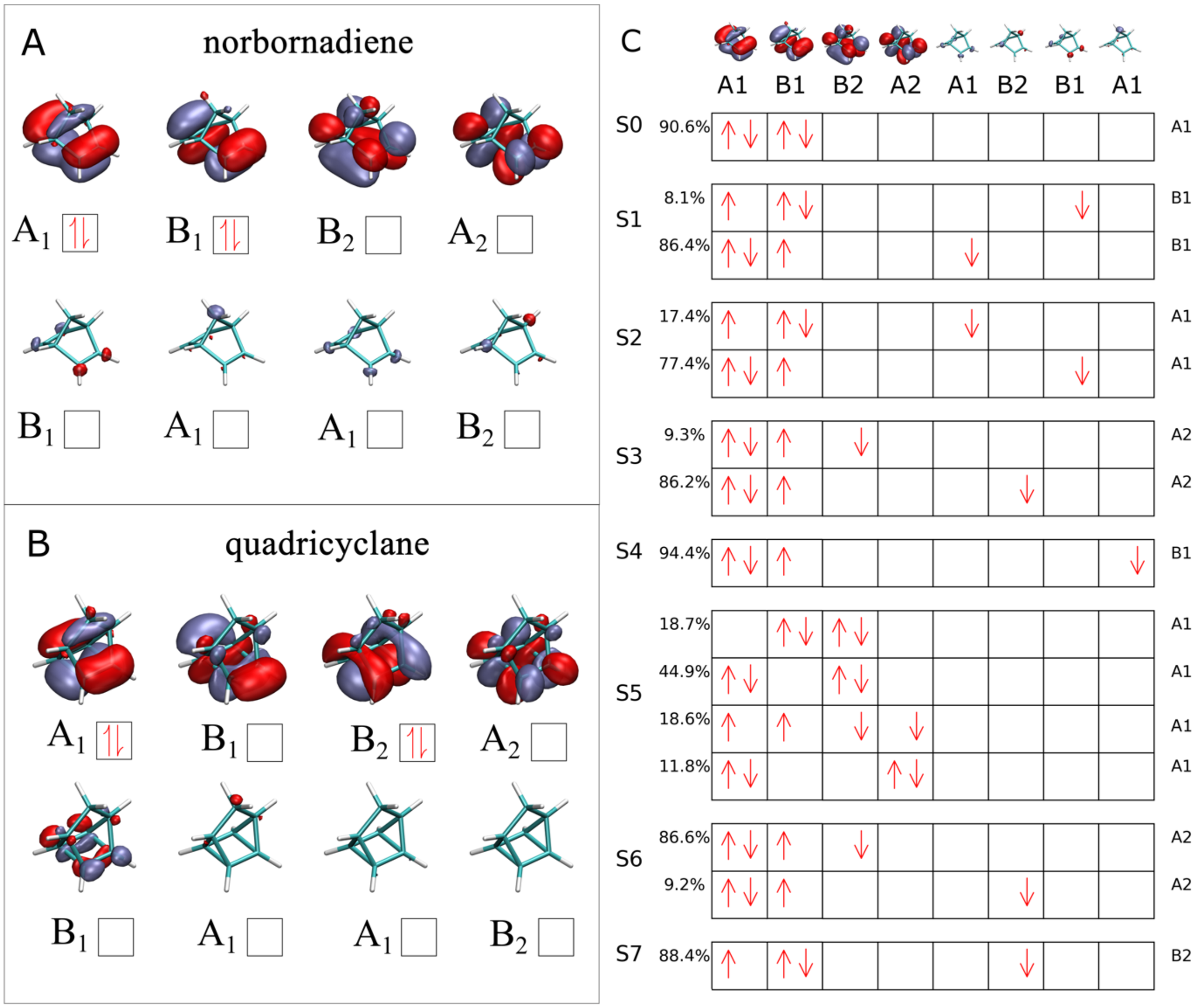

Figure S3. Active MO's and dominant electronic configurations. The 8 active MO's (3 A_1, 1 A_2, 2 B_1 and 2 B_2) in the norbornadiene (A) and quadricyclane (B) forms used in the SA(14) CASSCF(4,8)/AUG-CC-PVDZ electronic structure computations. Isocontour values of 0.04 Bohr^{-3}. Valence orbitals are shown in the top row and Rydberg ones in the bottom row. C Main configurations of the 7 lowest excited states at the norbornadiene equilibrium geometry computed at the SA(14) CASSCF(4,8)/AUG-CC-PVDZ level.

The excitation energies of the electronic states at the equilibrium geometries of norbornadiene, quadricyclane and of the MECI S_0/S_1 CI are given in Table S4.

Table S4. Energies in eV at the equilibrium geometries of norbornadiene, quadricyclane and at the minimum energy S_0/S_1 conical intersection.

	norbornadiene	MECI S_0/S_1	quadricyclane
S0	0.000	4.313	2.732
S1	5.815	4.318	7.484
S2	6.153	6.558	7.733
S3	6.321	7.078	7.892
S4	6.656	7.306	8.014
S5	7.537	7.674	8.504
S6	7.619	9.384	8.544
S7	7.694	9.650	9.171

There is a gap of about 6 eV in the norbornadiene Franck Condon region and 5 eV for the quadricyclane form between the ground state and a dense manifold of excited states of Rydberg and mixed valence-Rydberg character which are very close in energy in a range of 2-3 eV. Overall, the UV absorption averaged over the Franck-Condon region is in agreement with experimental results,[2, 3] as can be seen from the computed absorption spectrum (Figure 2E) shown in the method section of the main text. The determinantal composition of the 7 lowest excited states taken into account in the dynamical computations at the minimum energy of the norbornadiene form on the grid is reported in Figure S3C. The relative energetical order of Rydberg and valence states is very sensitive to the details of the electronic structure method. The determinantal composition of low lying excited states and their relative energetical order obtained at the SA-CASSCF level is different from that reported using CAS-SCF or CASPT2 with smaller active spaces. [2-5] Our active space was chosen so that we get a proper description of the band of 7 electronic states over the geometries span by the entire grid, including the quadricyclane product. The SA-CASSCF approach with uniform weights on the electronic states is known to overestimate the energies of the excited states and to have at best an accuracy in relative energies of 0.2-0.5 eV. In our computations, the $S_1(B_1)$ and S_2 (A_1) states have a mixed 3p and 3s Rydberg character and are optically active. Their excitation energies (5.85 eV and 6.15 eV) are in reasonable agreement with previous results.[2, 5] On the other hand, S_3 (A_2, 6.321 eV) has a mixed Rydberg - valence excitation character and is dark. In agreement with previous computations, we observed a low lying state formed with doubly excited determinants, the S_5 state (A_1, 7.537 eV). The diffuse lower excited valence (V2) state resulting from excitations from A1 to B2 MO's reported in refs. [2-4] is not present at the equilibrium geometry on our grid. We note however that we get low absorption below 5.85 eV in the absorption spectrum when we average over the grid points of the Franck Condon region (Figure 2E in the main text) as was observe experimentally.[2, 3, 6] In the open norbornadiene equilibrium geometry, and in general in the Franc-Condon region, S_3 , S_5 and S_6 (7.619 eV) exhibit excitations to the B_2 valence orbital which becomes the HOMO in the electronic configuration of the GS of quadricyclane, see Figure S3C. When the geometry is distorted along the θ and the γ coordinates, this excitation is transferred to lower excited states via non adiabatic interactions all the way down so that the corresponding configuration becomes the dominant one in the ground state of the closed quadricyclane form. Therefore, the quadricyclane configuration appears in the intermediate adiabatic excited states involved in the simulations (S_1, S_2, S_3 and S_4 (6.656 eV)) as the various conical intersections are approached by the wavepacket on the way to the quadricyclane region.

An approximate symmetry C_{2v} is preserved in the Franck Condon region of the open norbornadiene form. At the norbornadiene equilibrium geometry, the lower excited states can be assigned a symmetry based on the symmetry of the main configurations, as shown in Figure S3C. Optical selection rules of the C_{2v} group are therefore reflected in the values of the cartesian components of the transition dipoles gathered in Table S5. The x direction of the laboratory frame belongs to the B_1 irreducible representation, y to B_2 and z to A_1. The closed shell ground state belongs to A_1.

It would be ideal to access the S_3, S_5 or S_6 to obtain an efficient isomerization process. However, S_3 and S_6 have a A_2 symmetry which makes them dark upon UV excitation and they remain not very efficiently coupled to lower excited by transition dipoles in the Franck-Condon region. The state S_5 consists of double or quadruple excitations at the C_{2v} geometry of the norbornadiene equilibrium geometry. In the Franck-Condon region, its electronic structure remains complex. Outside of the Franck-Condon region, transition dipoles in the y direction are allowed because of the geometry distortion as can be seen from Table S6 which gives the values of the transition and permanent dipoles at the minimum energy of the S_0/S_1 conical intersection on the grid.

Table S5: x, y and z components of the transition dipole in a.u. between the excited states computed on the norbornadiene equilibrium geometry on the grid.

x	S0	S1(B$_1$)	S2 (A1)	S3 (A2)	S4 (B1)	S5 (A1)	S6(A2)	S7 (B2)
S0	0.00	-0.56	0.00	0.00	-0.14	0.00	0.00	0.00
S1	-0.56	0.00	-3.26	0.00	0.00	-0.05	0.00	0.00
S2	0.00	-3.26	0.00	0.00	0.12	0.00	0.00	0.00
S3	0.00	0.00	0.00	0.00	0.00	0.00	0.00	-2.11
S4	-0.14	0.00	0.12	0.00	0.00	-0.06	0.00	0.00
S5	0.00	-0.05	0.00	0.00	-0.06	0.00	0.00	0.00
S6	0.00	0.00	0.00	0.00	0.00	0.00	0.00	0.13
S7	0.00	0.00	0.00	-2.11	0.00	0.00	0.13	0.00
y	S0(A1)	S1(B1)	S2(A1)	S3(A2)	S4 (B1)	S5 (A1)	S6 (A2)	S7 (B2)
S0	0.00	0.00	0.00	0.00	0.00	0.00	0.00	0.23
S1	0.00	0.00	0.00	3.91	0.00	0.00	-1.06	0.00
S2	0.00	0.00	0.00	0.00	0.00	0.00	0.00	-1.79
S3	0.00	3.91	0.00	0.00	-0.35	0.00	0.00	0.00
S4	0.00	0.00	0.00	-0.35	0.00	0.00	0.60	0.00
S5	0.00	0.00	0.00	0.00	0.00	0.00	0.00	-0.16
S6	0.00	-1.06	0.00	0.00	0.60	0.00	0.00	0.00
S7	0.23	0.00	-1.79	0.00	0.00	-0.16	0.00	0.00
z	S0(A1)	S1(B1)	S2(A1)	S3(A2)	S4(B1)	S5(A2)	S6(A2)	S7(B2)
S0	0.28	0.00	-0.47	0.00	0.00	-0.05	0.00	0.00
S1	0.00	0.94	0.00	0.00	3.33	0.00	0.00	0.00
S2	-0.47	0.00	0.97	0.00	0.00	0.01	0.00	0.00
S3	0.00	0.00	0.00	0.45	0.00	0.00	0.29	0.00
S4	0.00	3.33	0.00	0.00	-2.04	0.00	0.00	0.00
S5	-0.05	0.00	0.01	0.00	0.00	0.35	0.00	0.00

S6	0.00	0.00	0.00	0.29	0.00	0.00	0.08	0.00
S7	0.00	0.00	0.00	0.00	0.00	0.00	0.00	0.53

Table S6. x, y and z components of the transition dipole in a.u. between the excited states computed at the geometry of the minimum energy S_0/S_1 CI on the grid.

x	S0	S1	S2	S3	S4	S5	S6	S7
S0	0.00	0.00	-0.62	0.00	0.64	0.00	-0.01	0.04
S1	0.00	0.00	-0.93	0.00	0.52	0.01	0.00	0.01
S2	-0.62	-0.93	0.01	-0.62	0.02	-3.08	-0.97	-0.40
S3	0.00	0.00	-0.62	-0.01	-0.25	0.00	0.00	0.00
S4	0.64	0.52	0.02	-0.25	-0.01	1.44	0.03	0.16
S5	0.00	0.01	-3.08	0.00	1.44	0.01	0.00	0.00
S6	-0.01	0.00	-0.97	0.00	0.03	0.00	-0.01	-0.04
S7	0.04	0.01	-0.40	0.00	0.16	0.00	-0.04	0.18
y	S0	S1	S2	S3	S4	S5	S6	S7
S0	0.00	0.00	-0.04	0.00	0.38	0.00	-0.01	-0.02
S1	0.00	0.00	0.01	0.00	0.15	0.00	-0.01	-0.01
S2	-0.04	0.01	-0.01	3.83	0.01	-0.77	0.10	-0.08
S3	0.00	0.00	3.83	0.03	-1.54	-0.01	0.00	0.00
S4	0.38	0.15	0.01	-1.54	-0.10	0.58	-0.21	-0.02
S5	0.00	0.00	-0.77	-0.01	0.58	-0.02	-0.01	0.00
S6	-0.01	-0.01	0.10	0.00	-0.21	-0.01	0.00	0.04
S7	-0.02	-0.01	-0.08	0.00	-0.02	0.00	0.04	-0.11
z	S0	S1	S2	S3	S4	S5	S6	S7
S0	-0.26	-0.04	-0.01	0.20	0.00	-0.17	0.32	-0.19
S1	-0.04	-0.07	0.00	0.01	0.00	-0.09	0.10	-0.08
S2	-0.01	0.00	2.47	-0.01	2.83	0.02	-0.01	-0.01
S3	0.20	0.01	-0.01	1.14	-0.02	-0.05	0.01	0.03
S4	0.00	0.00	2.83	-0.02	-2.09	-0.02	0.00	0.00
S5	-0.17	-0.09	0.02	-0.05	-0.02	0.29	0.23	-0.05

S6	0.32	0.10	-0.01	0.01	0.00	0.23	-0.62	-0.03
S7	-0.19	-0.08	-0.01	0.03	0.00	-0.05	-0.03	2.75

Based on the C_{2v} selection rules, as explained in the main text, we have chosen to use an excitation by a UV fs pulse polarized along x and resonant with the S_1 (B1) which we call UV(x) and a UV fs pulse polarized along z and resonant with the S_2 (A_1) state which we call UV(z). For the UV(x) pulse, the S_1 wavepacket that is formed upon excitation exhibits a Rydberg character, and the conical intersection S_1/S_0 is reached after a large oscillation along the coordinates θ and γ.
The UV(z) is tuned to excite S_2 which is strongly coupled to the dark S_3 state in the Franck-Condon region. The UV(z) excitation therefore builds a wavepacket that is a superposition of two Rydberg states that exhibit densities along x (S_2, see Figure S3C) and y (S_3 see Figure S3C), which are the directions of the new and the old bonds respectively. Compared to the UV(x) excitation, the UV(z) excitation lead to a very different path for the quantum dynamics. The electronic density resulting from a superposition of the S_2 (x Rydberg) and S_3 (y Rydberg) states is delocalized along the x and y spatial directions, leading to a weakening of the old bond (along y) and formation of the new one (along x). At the exit of the Franck-Condon region the potentials of the S_2 and the S_3 states are such that the electronic coherence moves along θ, rapidly approaching the region of the grid where the product determinantal character of higher states begins to mix with the S_2 and the S_3 states.

2.2 Non Adiabatic Couplings

The spatial localization of the Non Adiabatic Coupling (NAC) elements in the three-dimensional grid is quite different for different pairs of coupled electronic states. The spatial extent and the strength of the NAC depend on how well the geometry distortions at the conical intersection seams is captured by the three coordinates that we selected. Obviously, we cannot capture all the NAC regions equally well with only three coordinates. Our coordinates system allows to capture well the S_0/S_1 and S_2/S_3 non adiabatic interactions (see Figure S4A and B for the displacements corresponding to the gradient difference and the NAC vectors [7] at the geometry of the minimum energy conical intersection for S_0/S_1 and S_2/S_3 respectively). Isocontours of their magnitude on the 3D grid are shown in Figure S5 in grey shadings. One can see that their localization patterns are quite different. The S_0/S_1 intersection is very localized on a diagonal in the region of positive values for γ , θ and φ. On the other hand, the S_3/S_2 NAC coupling is instead present in a very large region that goes all the way from the Franck-Condon region to the center of the cube. As explained in the main text, the S_2/S_1 non adiabatic interactions are not well captured in our coordinate system, as can be seen for the displacements of the NAC vector shown in Figure S4C.

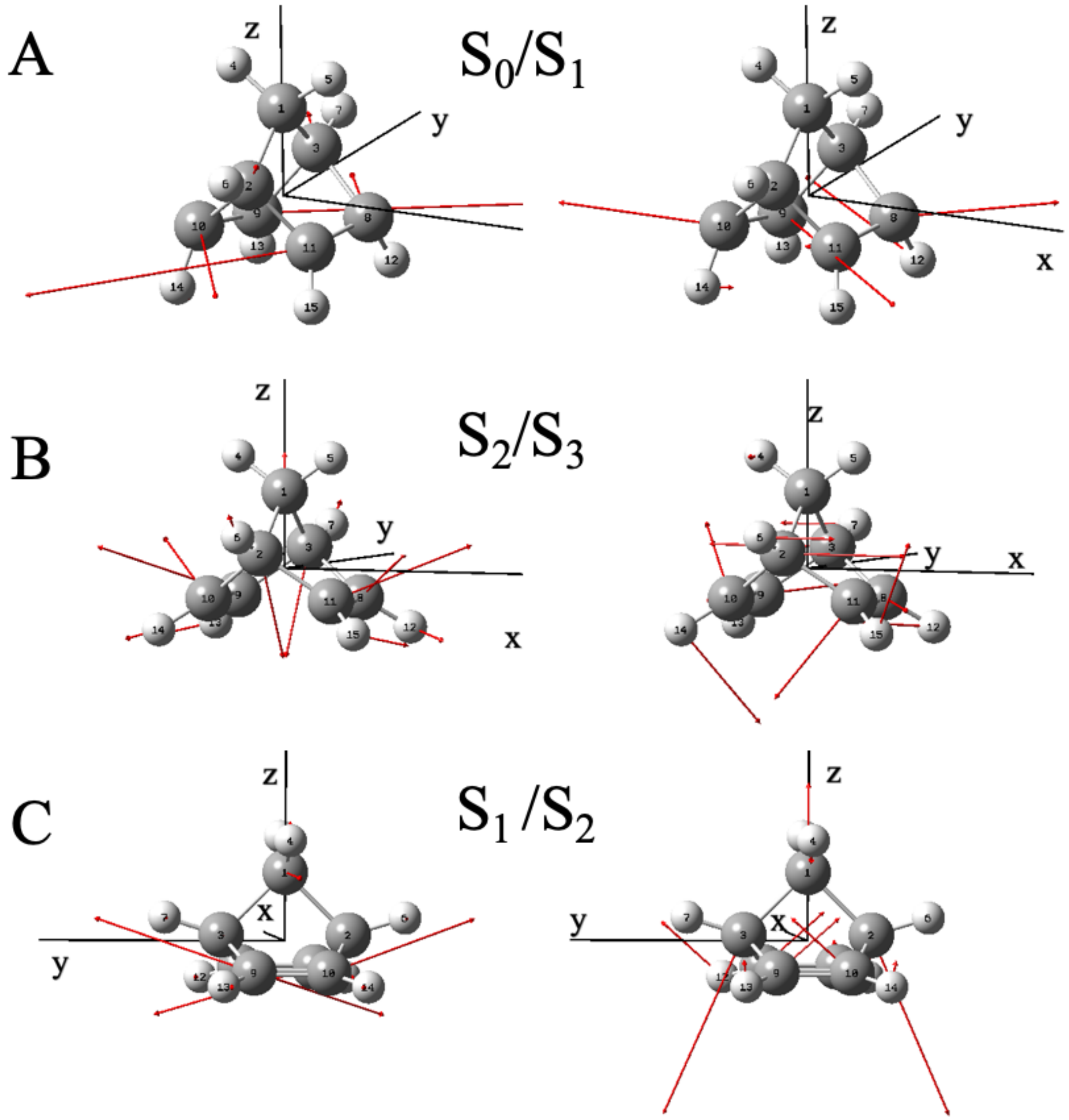

Figure S4: Gradient difference (left) and NAC (right) vectors for important conical intersections. A: S_0/S_1 minimum energy conical intersection, B: S_2/S_3 minimum energy conical intersection. C: S_1/S_2 minimum energy conical intersection

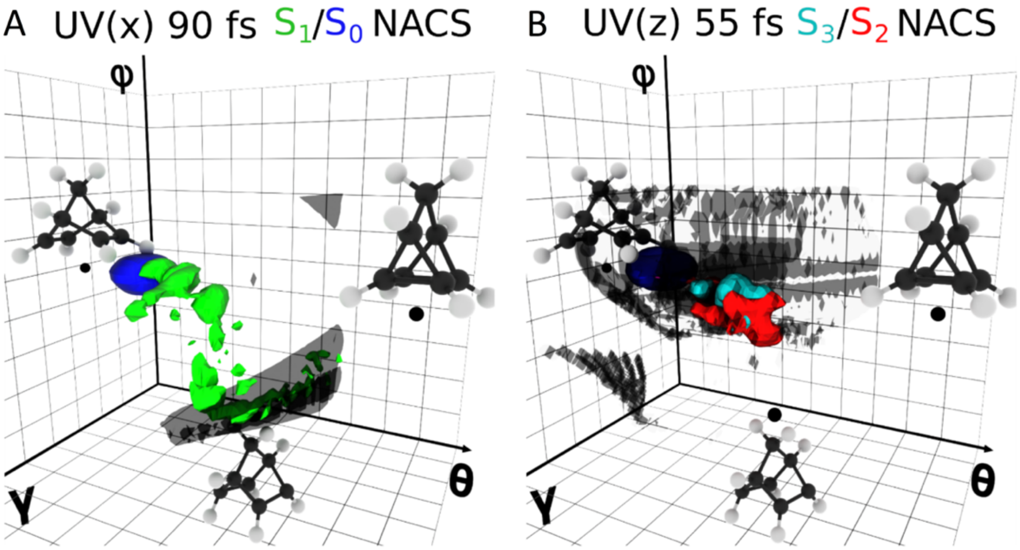

Figure S5. Isocontours of important non adiabatic couplings. A) Isocontours (±0.00001 bohr^{-3}, grey shading) of the S_0/S_1 non adiabatic coupling. The isocontour (0.0001 bohr^{-3}) of the spatial localization of the wavepacket on S_0 (blue) and on S_1 (green) computed for the UV(x) simulation at 90 fs is also shown. The non adiabatic coupling region is very localized in the positive corner of the γ , θ and φ grid. B) Isocontour (±0.00001 bohr^{-3}) of the S_2/S_3 non adiabatic coupling; it is worth remarking how much more spread it is compared to the S_0/S_1 one. Also shown is an isocontour (0.0001 bohr^{-3}) of the spatial localization of the wavepacket on S_2 (red) and on S_3 (turquoise) computed for the UV(z) simulation at 55fs.

2.3 Consistency of the phase of the electronic state wave functions across the grid.

In the matrix diagonalization of the SA-CASSCF, the eigenvector wave function is defined up to a sign at every grid point since the wave function is real. This is usually not a problem for the potential energies and in general diagonal values of operators. However, for the transition dipole and the non adiabatic coupling elements which depend on the wave function of two eigenstates, the sign needs to be consistent across the grid. We implemented a sign correction procedure in order to impose consistency of the sign of the wavefunction and avoid purely numerical jumps of π in their phase between adjacent points . The algorithm is based on state overlaps between two neighboring geometries to detect root swaps and correct the phase changes, taking as a reference the minimum energy structure and propagating the correction along the three coordinates.

S3 Quantum dynamics

3.1 Hamiltonian and integration of the TDSE in θ,γ and φ coordinates

The kinetic energy and momentum operator in the θ,γ and φ coordinates have been derived starting from Cartesian coordinates using the general expression.[8, 9]} The kinetic energy operator is a sum of nine terms:

$$\hat{T} = \hat{T}_{\theta\theta} + \hat{T}_{\gamma\gamma} + \hat{T}_{\varphi\varphi} + \hat{T}_{\theta\gamma} + \hat{T}_{\gamma\theta} + \hat{T}_{\theta\varphi} + \hat{T}_{\varphi\theta} + \hat{T}_{\gamma\varphi} + \hat{T}_{\varphi\gamma} \tag{S4}$$

Each element in Eq. (S4) takes the form

$$\hat{T}_{wu} = \frac{1}{2}\left(\tilde{g}^{-1/4}\hat{p}_w^{\dagger}\left[G_{wu}\tilde{g}^{1/2}\hat{p}_u\tilde{g}^{-1/4}\right]\right) \tag{S5}$$

where w and u = θ,γ and φ. $\tilde{g}$ is the determinant of the 3x3 matrix $\mathbf{g}$ of the mass weighted Cartesian coordinates derivatives obtained from Eqs. (S2) and (S3) with respect to θ,γ and φ and **G** is its inverse. The matrix elements of **g** can be computed analytically from Eqs. (S2) and (S3) and **g** is of rank 3, so that its inverse **G** is non singular. $\hat{p}_u = \frac{\hbar}{i}\hat{\nabla}_u$, u= θ,γ , φ is the momentum operator.

In order to keep the simulation numerically stable, we extended the system boundaries by adding 30 points at each side along the θ coordinate (leading to a total of 30+100+30=160 points), 15 along each side of γ (15+26+15=56 points in total) and 15 along each side of φ (15+25+15=55 points in total). In the extended grid region, the values of the potential energies have been 3D extrapolated, and all the NAC elements and transition dipole moments are set to 0. The time dependent Schrödinger equation is integrated numerically for N=8 coupled electronic states and N_g = 492800 grid points.

$$i\frac{dc_{ig}(t)}{dt} = \sum_{j=1}^{N}\sum_{g'=1}^{N_g} H_{ig,jg'}\,c_{jg'}(t) \tag{S6}$$

Atomic units are used throughout. The Hamiltonian includes the non adiabatic coupling between the electronic states and the dipole coupling. Its matrix elements between two basis wave functio $|ig\rangle$ and $|jg'\rangle$ take the form:

$$\mathbf{H}_{ig,jg'}(t) = -\frac{1}{2}\mathbf{T}_{ig,jg'}\delta_{ii} + \mathbf{V}_{ig,jg'}\delta_{ij}\delta_{gg'} - \mathbf{E}(t)\cdot\mu_{ig,jg'}\delta_{gg'} + \left(\frac{1}{i}\tau_{ig,jg}\delta_{gg'}\right).\mathbf{p}_{jgg'} \qquad \text{(S7)}$$

where i and j stand for the electronic state index and g and g' for the grid index, that is a value of θ, γ and φ. $\mathbf{T}_{ig,jg'}$ are the matrix elements of the kinetic energy operator defined in Eq. S4 and S5 above, which are diagonal in the electronic state index. The momentum operator, $\hat{p}_u$, is a Hermitian operator. The matrix elements of the momentum operator (see definition below Eq. S5), are also diagonal in the electronic state index when it operates on the grid nuclear coordinate. They are computed using a finite difference algorithm[10, 11] as explained below. The matrix elements of the momentum operator acting on the nuclear coordinate of the adiabatic electronic state, $\frac{1}{i}\hat{\nabla}_u$, are off diagonal in the electronic index and diagonal in the grid index. The matrix elements $\tau_{ig,jg} = \langle i|\hat{\nabla}_u|j\rangle_g$ are computed at each grid point, using the quantum chemistry program OpenMolcas. We neglect in Eq. S7 the second derivative matrix elements with respect to the nuclear coordinate of the electronic wave function. $\mathbf{V}_{ig,jg'}$ are the matrix elements of the potential energy, diagonal in both the electronic and grid indexes. The potential energy is computed for each grid point as described in Section S2. As stated above, the equilibrium quadricyclane form on S_0 is not inside the 3D grid. In order to estimate quadricyclane yield, we add an absorbing potential, $-iA_g$, on the quadricyclane side for high values of the θ coordinate (see Figure S6D below), on each electronic state whose dependence on θ is parametrized as:

$$A_g = a\left(-\arctan\left(b(\theta + c) + d\right)\right) \qquad \text{(S8)}$$

where a is the highest value of the potential (set to 0.5 a.u. or 15 eV), b=1000 is the steepness factor for the arctan function, c=-0.7 is the flex position with respect to θ and d=-1.55548 is the shifting factor that we chose to make the function larger than zero only in the extrapolation part of the cube.

In Eq. (S7), $\mu_{ig,jg'}$ is the dipole moment vector, diagonal in grid points, in the three Cartesian coordinates of the laboratory frame. The terms diagonal in the electronic index represents the permanent dipole moments and the off diagonal ones the transition dipoles. $\mathbf{E}(t)$ is the time-dependent vector of the electric field of the pulse in the laboratory frame. $\mathbf{E}(t)$ is defined from the time-derivative of the vector potential to ensure that the time integral of the electric field is zero.

$$\mathbf{E}(t) = -\frac{d\mathbf{A}(t)}{dt} = \varepsilon f_0 \exp\left[\frac{-\left(t-t_0\right)^2}{2\sigma^2}\right]\left(\cos\left(\omega\left(t-t_0\right)+\phi\right) - \frac{\sin\left(\omega\left(t-t_0\right)+\phi\right)\left(t-t_0\right)}{\omega\sigma^2}\right) \tag{S9}$$

where ω is the carrier frequency, f_0 the field strength, σ the pulse duration (FWMH=2.35 σ), ε is the polarization vector and ϕ is the carrier envelope phase (CEP), i.e. the phase between the electric field of the pulse and the gaussian envelope.

The last term in Eq. (S7) is the non adiabatic coupling between electronic states *i* and *j*. $\tau_{ig,jg}$ is the non adiabatic coupling vector expressed in the coordinates θ,γ and φ, diagonal in grid points and $\mathbf{p}_{jgg'}$ is the matrix of the vector of the momentum operator on state *j* in the coordinates θ,γ and φ, $\hat{p}_u = \frac{\hbar}{i}\hat{\nabla}_u$, *u*= θ,γ, φ. We neglect the second derivative terms of the non adiabatic coupling in the dynamical computations.

In order to be able to numerically implement the integration of the time-dependent Schrödinger equation for a vector of amplitudes of 8 x 492800 complex numbers, we compute the action of the non local kinetic energy and momentum operators using a finite difference scheme with $O\left(h^4\right)$ error.[10, 11]

The first-order derivatives are computed as [12]

$$\frac{dc_{u,v,w}}{du} = \frac{1}{du}\left(\frac{1}{12}c_{u-2,v,w} - \frac{3}{2}c_{u-1,v,w} + \frac{3}{2}c_{u+1,v,w} - \frac{1}{12}c_{u+2,v,w}\right) \tag{S10}$$

where *u, v, w* represents the three coordinates corresponding to a grid point *g;* the electronic indexes are omitted since the momentum and kinetic energy operators are diagonal in the electronic index. The second order derivatives are given by:

$$\frac{d^2 c_{u,v,w}}{du^2} = \frac{1}{12du^2}\left(-c_{u-2,v,w} + 16c_{u-1,v,w} + 30c_{u,v,w} - 16c_{u+1,v,w} - c_{u+2,v,w}\right) \qquad \text{(S11)}$$

and the cross derivatives between two internal coordinates *v* and *u:*

$$\frac{dc_{u,v,w}}{dvdu} = \frac{1}{2dvdu}\left(-c_{u,v+1,w} - c_{u,v-1,w} - c_{u+1,v,w} - c_{u-1,v,w} + c_{u-1,v-1,w} + c_{iu+1,v+1,w} + 2c_{u,v,w}\right)$$

The amplitudes $c_{ig}\left(t\right)$ are propagated using Eq. (S6) using a time step of 10 as, and a 4th order Runge-Kutta scheme for the time integration.

The dynamics is started from the ground vibrational state of the ground electronic state, which is determined using a harmonic approximation for each coordinate. The numerically determined harmonic frequencies and the corresponding periods in the three coordinates are 479.5 cm^{-1} (69.5 fs) for θ, 1550.7 cm^{-1}(21.5 fs) for γ and 936.5 cm^{-1} (35.6 fs) for φ.

The population in each electronic state, *i*, is computed by summing the square modulus of the amplitudes $\left|c_{ig}\left(t\right)\right|^2$ over all the N_g = 492800 grid points:

$$P_i\left(t\right) = \sum_{g=1}^{Ng} \left|c_{ig}\left(t\right)\right|^2 \qquad \text{(S12)}$$

S4 Additional details on the quantum dynamics

4.1 Partitioning of the grid space

The configurational space spanned by the 3D grid on the ground state is partitioned in three regions based on the localization of the S_0/S_1 coupling shown in Figure S6C below. We define a 'reactant' region which corresponds to an overall norbornadiene geometry, a 'product' region that corresponds to a quadricyclane one and a 'undecided' region where the distortion of the geometry does not allow to attribute a norbornadiene or a quadricyclane character. After its transition from S_1 to S_0, a wavepacket localized in the green portion of the cube will eventually get absorbed by the imaginary potential and is defined as a 'product'. A wavepacket on S_0 localized in the yellow region will never reach the absorbing potential and is counted as 'reactant'. A large fraction of the

S_0 wavepacket typically remains localized in the Franck-Condon region and is counted as "undecided".

4.2 Dynamics in the vicinity of the S_0/S_1 conical intersection

The dynamics on the S_1 state in the vicinity of the S_1/S_0 conical intersection region determines the yields on S_0 of 'product' or 'reactant' configurations. In order to better understand how to control this yield, we have carried out five simulations of a wavepacket defined as the norbornadiene ground vibrational wavepacket on S_0 but localized on S_1 at five different initial localizations around the S_0/S_1 conical intersection, see Figure S6A. We obtain quite different final yields that clearly depend on how the wavepacket on S_1 approaches the conical intersection region. This analysis allowed us to determine by back integration from the most advantageous position in product yield what are the ideal initial conditions in the Franck- Condon region and consequently design the UV(z) pulse. We summarize below the essential features of the dynamics resulting from the five different initial localizations. A schematic initial localization of the 5 initial wavepackets is shown in Figure S6A and isocontours of the wavepacket on S_1 at t=0 and on S_1 and S_0 at t=50 fs in Figure S7. The population time evolution of the populations on S_0 and S_1 is shown and the yields in reactants and products in Figure 6D.

Localization 1 corresponds to an initial wavepacket on S_1 very close to the conical intersection, with same θ and φ values and a slightly larger value of γ (i.e. less double bond character), see Figure S6A and Figure S7. Consequently, 15% of the population is transferred to S_0 in the first 10 fs.; then the wavepacket quickly leaves the conical intersection region. The product/reactant ratio of this simulation is extremely low. In the first passage through the conical intersection, virtually the entire population goes back to the reactant, see Figure 7B.

Localization 2 also corresponds to an initial wavepacket very close to the conical intersection with same θ and φ values, but with smaller values of γ (more double bond character), so that it is localized on the other side of the conical intersection, see Figure S6A and Figure S7. The amount of population transfer is not as immediate as in **1**, but it is slowly increasing, without a particularly high product/reactant ratio, Figure S6D. At the end of the 50 fs, these initial conditions are the ones leading to the smallest transfer of population and smallest product yields (3:1 reactants/products) because the wavepacket remains trapped in the vicinity of the initial region, see Fig. S7.

Localization 3 corresponds to an initial wavepacket with smaller values of θ (closer to the open quadricyclane form), smaller values of γ and smaller values of φ, see Figure S6A and Figure S7. Most of the population in S_1 moves to high value of γ and approaches the conical intersection with an angle similar to **1**. The population transfer is (at least in the first 20 fs) very selective towards the product (90%) and it has a second passage which is also very selective towards products (70%), see Figure S7B.

Localization 4 corresponds to an initial wavepacket in a region where the NAC between S_1/S_2 is high, see Figure S6A and Figure S7A. The θ values are the same as **1** and **2**, the wavepacket is basically localized at the CI, but γ and φ are both closer to zero. In the first passage the population transfer is very selective towards the product, with a first passage that goes in the direction of elongating γ which gives basically 100% selectivity, see Figs. S6D and S7B.

Localization 5 corresponds to an initial wavepacket on S_1 gliding in a way similar to the one followed by the wavepacket in the UV(x) simulation. It has not a good selectivity towards the product in the first passage and the second one (2:1 reactants/products), see Figs. S6D and S7B.

In summary, as shown in Figs. S6 and S7, at the first passage of the wave packet through the conical intersection region, the best efficiency to the product is found to be from initial position **4**. We then back-integrated the wave packet on S_1 from this position to the reactant region, obtaining in the Franck Condon region a coherent superposition of the S_2 and S_3 electronic states, which can only be accessed by a UV pulse polarized on the z direction. On the other hand, initial position **1** (see Figs. S6 and S7) essentially corresponds to the path followed by a vibronic wave packet produced on S_1 by a short UV pulse polarized on the x direction and is less efficient for population transfer to the quadricyclane region.

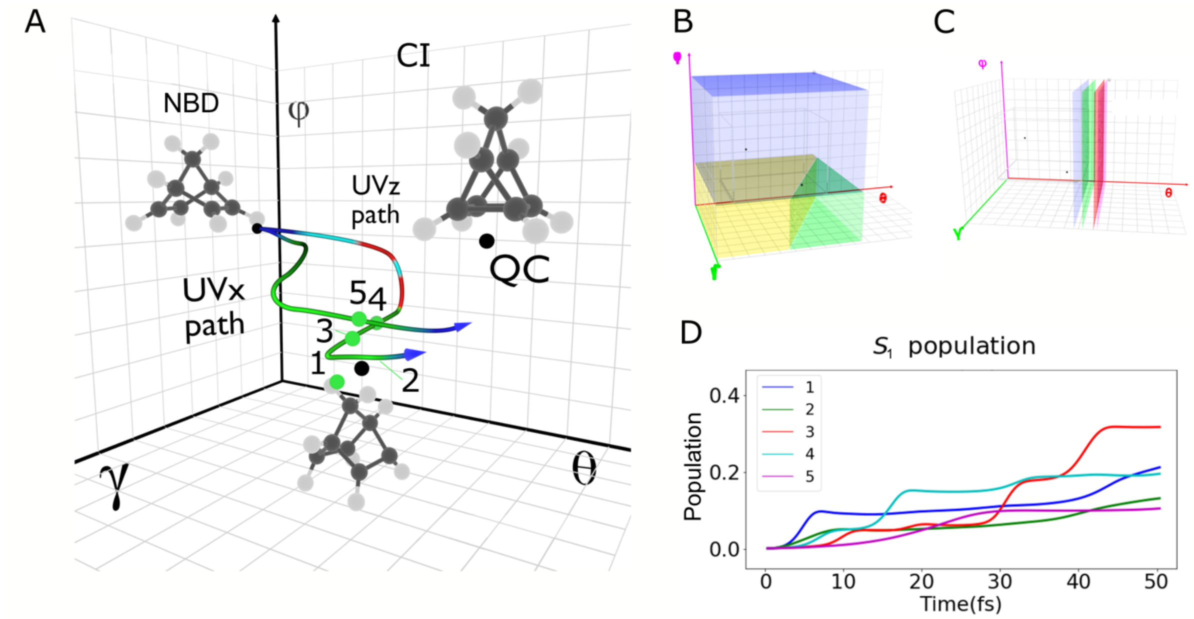

Figure S6: Paths around the S_0/S_1 conical intersection. A) The 5 different initial localizations of the wavepacket on S1 around the S_0/S_1 conical intersection. The red line corresponds to the path followed by the non stationary wavepacket corresponds to an excitation of the norbornadiene ground state by the UV(z) pulse and passes by localization **4**. The green line corresponds to the wavepacket followed by the UV(x) excitation of the norbornadiene ground state and passes by position **5**. B) The partition of the 3D grid into a 'product' region (green), a 'reactant' region (yellow) and an 'undecided' region (blue). C) the (γ,φ) planes of the absorbing imaginary potential at large values of the θ coordinate, see Eq. (S8). D) Population on the S_1 state for the 5 simulations.

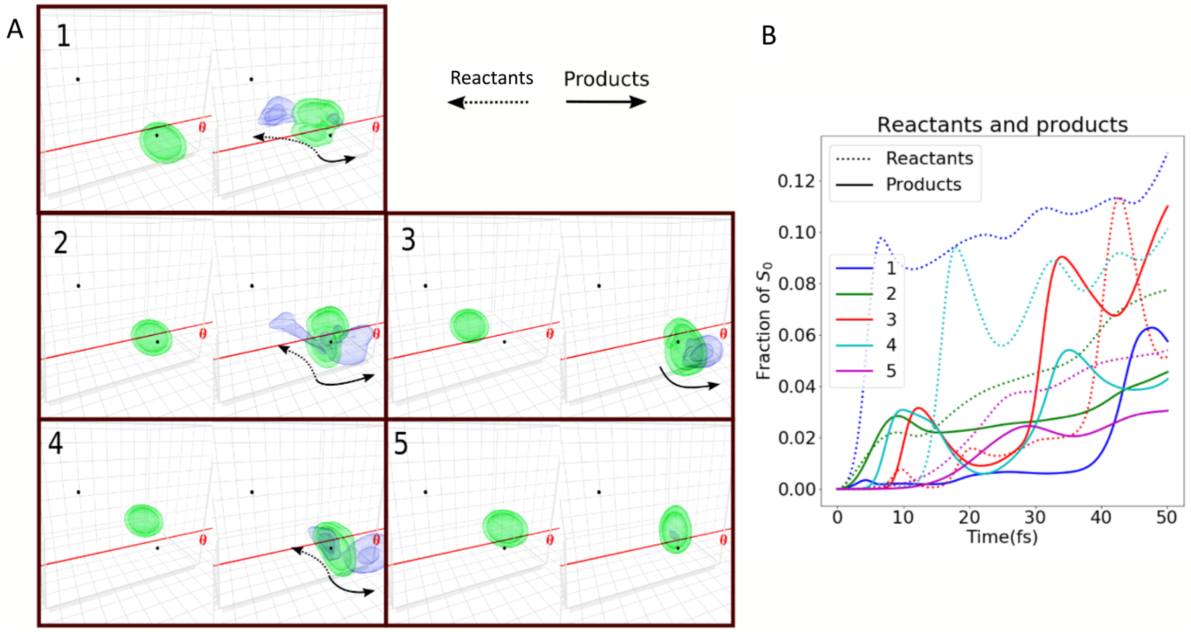

Figure S7: Selectivity of different paths around the conical intersection. A) The initial (t=0 fs, left panel) and final (t=50 fs, right panel) localization of the wavepacket on S_1 (green) and on S_0 (blue) for the 5 initial positions as indicated. B) Population in reactants and products for the five initial conditions.

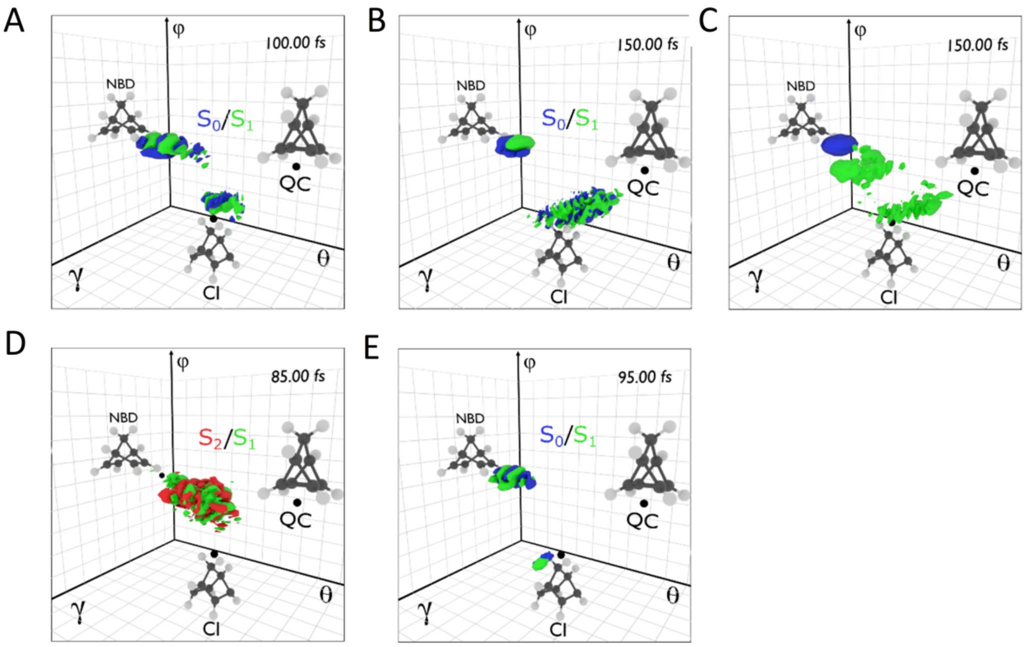

Figure S8**:** Complementary snapshots of the wave packet localization for the UV(x) and UV(z) excitation. Panels A, B, and C: snapshots of longer time evolution of the S_1 wave packet created by the UV(x) pulse as it revisits the conical intersection region with a period of 50 fs: isocontour of the S_0/S_1 coherence at the second passage (t=100 fs, panel a) and third passage (t=150 fs, panel b). Panel c shows the localization of the S1 and S0 wavepackets. Isocontour values (0.0001 bohr^{-3} for a,b and 0.001 for c)**.** panels D and E: snapshots of the coherences resulting from the UV(z) excitation at 85 fs when the S_2/S_3 coherence (panel F of Figure 3 of the main text) reaches the S_2/S_1 CI which leads to a S_2/S_1 coherence (panel E) in addition to the S_2/S_3 one and at 95 fs (panel D) to a transfer to S_0 from S_1 in the product region. Isocontour values of 0.0001 bohr^{-3}.

4.3: **Computation of the non stationary electronic density along the four C-C bonds**

For each grid point *g*, there is a molecular geometry and corresponding one electron stationary electronic densities for each electronic state, $\rho_{ii,g}\left(x,y,z\right)$, and electronic transition density $\rho_{ij,g}\left(x,y,z\right)$ where *x*, *y* and *z* are the three Cartesian electronic coordinates and *i* and *j* the index of the electronic states. For each grid point *g*, one can therefore define non-overlapping volumes around the old bonds, i.e. the C-C of the ethylene moiety in the open norbornadiene form and around the new C-C bonds, i.e. the two new bonds formed by the ring closure to get quadricyclane. These volumes are shown in Figure 5 panel C. Integration of the total electronic density at a given time *t* gives the amount of electronic density on the 'old' and 'new' bonds along the quantum dynamics. The electronic density in a given bond volume at time *t* is given by:

$$\rho_{bond}^{elec}\left(t\right)=\sum_{i,j}^{N}\sum_{g} c_{ig}^{*}\left(t\right)c_{jg}\left(t\right)\rho_{ij,g}^{elec,bond} \qquad \text{(S13)}$$

The sum of electronic terms in Eq. (S13) can be separated into a diagonal term which corresponds to a population contribution to the electronic density in each type of bond and a coherence term, off diagonal in the electronic index:

$$\rho_{pop-bond}^{elec}(t) = \sum_{i}^{N} \sum_{g} \left| c_{gi}(t) \right|^2 \rho_{ii,g}^{elec,bond} \tag{S14}$$

$$\rho_{coh-bond}^{elec}(t) = \sum_{i \neq j}^{N} \sum_{g} c_{gi}^{*}(t) c_{gj}(t) \rho_{ij,g}^{elec,bond} \tag{S15}$$

The electronic density in a given bond type for the geometry of point g is:

$$\rho_{ij,g}^{elec,bond} = \sum_{x,y,z}^{bondtype} \rho_{ij,g}^{elec}(x,y,z) \tag{S16}$$

where the bond type corresponds to the volume of the 'red' or the 'blue' cylinders shown in Figure S8. The electronic one electron densities are computed in the basis of the natural molecular orbitals $\phi_m(\mathbf{r})$ obtained from the SA-CASSCF computation:

$$\rho_{ij,g}^{elec}(\mathbf{r}) = \sum_{m,n} \rho_{ij,g}^{nm} \phi_m(\mathbf{r}) \phi_n(\mathbf{r}) \tag{S17}$$

The two non-overlapping volumes corresponding to these pseudocylinders are defined as follows. For each geometry defined by the grid point *g*, two specific volumes encompassing the old and the new C-C bonds are defined.

These non-overlapping bond volumes are a sum of volume elements d*x*d*y*d*z* centered on a vector **r** that obey the following conditions: a point in space is considered part of the set of volume elements that define the new bond volume if it satisfies all the 5 conditions of the equation below. The first two conditions select the right quadrant, while the rest of the condition select the cylinder area between the two selected carbons. The result is a partition of space where the new and old bond cylinders are non-overlapping.

New bonds (blue cylinders), see Figure S1 for the atom numbering

$$\{\mathbf{r} : \mathbf{r} \,.\, \mathbf{N}_1 > 0\} \cap \{\mathbf{r} : \mathbf{r} \,.\, \mathbf{N}_2 < 0\} \cap \{\mathbf{r} : |\mathbf{r} \,.\, \mathbf{w}| < R\} \cap \{\mathbf{r} : \mathbf{r} \,.\, \mathbf{M}_1 > 0\} \cap \{\mathbf{r} : \mathbf{r} \,.\, \mathbf{M}_2 < 0\} \tag{S18}$$

where

- $\mathbf{N}_1$ is the normal vector to the plane defined by C1, C8 and C10
- $\mathbf{N}_2$ is the normal vector to the plane defined by C1, C9 and C11
- *R* is the cylinder radius (set to 1.4 Å).
- **B** is the vector connecting C10 and C11
    - $|\mathbf{r} \cdot \mathbf{w}|$ is the distance between **r** and **B**
    - $\mathbf{M}_1$ is the normal vector to the plane orthogonal to **B** that contains C10
    - $\mathbf{M}_2$ is the normal vector to the plane orthogonal to **B** that contains C11

Old bond (red cylinders)

$$\left\{\mathbf{r} : \mathbf{r} \,.\, \mathbf{N}_1 > 0\right\} \cap \left\{\mathbf{r} : \mathbf{r} \,.\, \mathbf{N}_2 < 0\right\} \cap \left\{\mathbf{r} : \left|\mathbf{r} \,.\, \mathbf{w}\right| < R\right\} \cap \left\{\mathbf{r} : \mathbf{r} \,.\, \mathbf{M}_3 > 0\right\} \cap \left\{\mathbf{r} : \mathbf{r} \,.\, \mathbf{M}_4 < 0\right\}$$

where

- $\mathbf{N}_1$ is the normal vector to the plane defined by C1, C8 and C10
- $\mathbf{N}_2$ is the normal vector to the plane defined by C1, C9 and C11
- *R* is the cylinder radius (set to 1.4 Å).
- **C** is the vector connecting C8 and C11
    - $|\mathbf{r} \cdot \mathbf{w}|$ is the distance between **r** and **C**
    - $\mathbf{M}_3$ is the normal vector to the plane orthogonal to **C** that contains C8
    - $\mathbf{M}_4$ is the normal vector to the plane orthogonal to **C** that contains C11

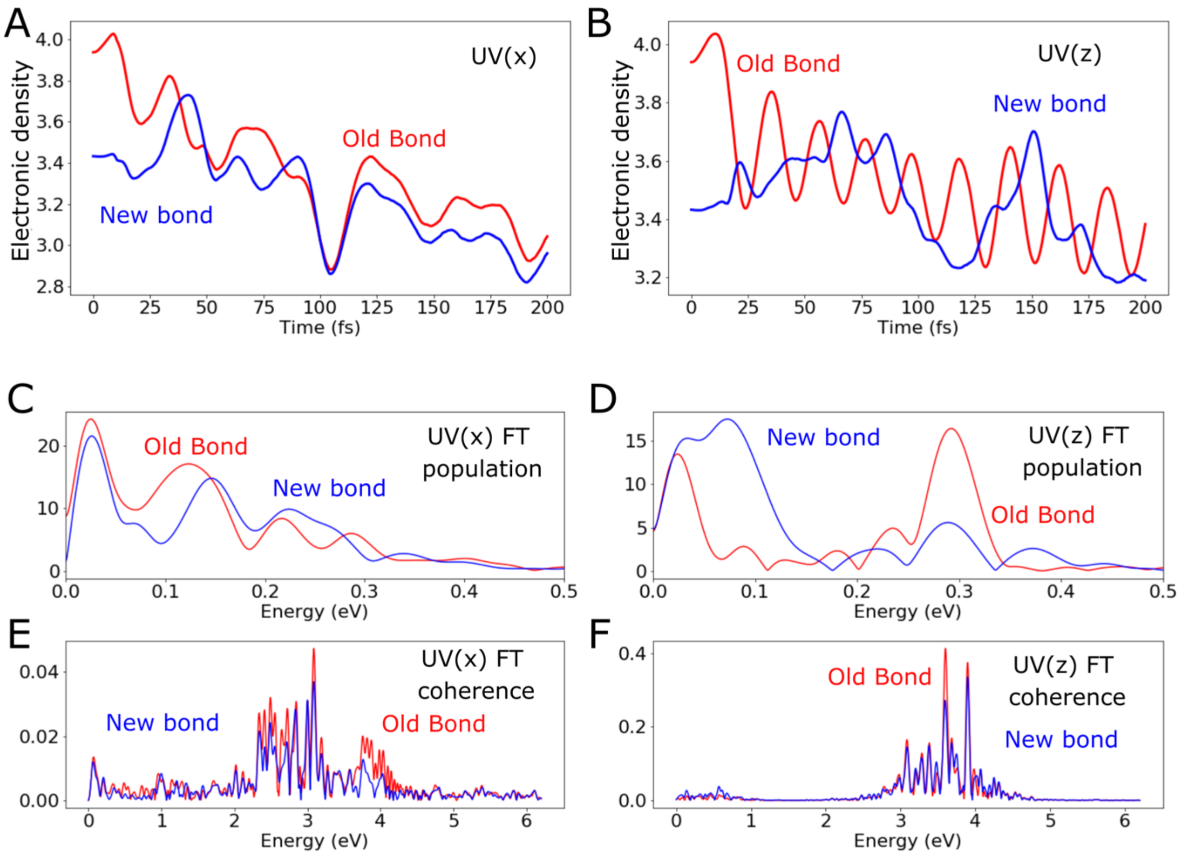

Figure S9: Electronic densities in the old and new bonds computed as a function of time for the UV(x) simulation (panel A) and for the UV(z) simulation (panel B). The overall decrease is due to the amount of population absorbed by the imaginary potential localized on the product side of the grid. Normalized densities are shown in Figure 5 of the main text. C) and D) FT of population terms of the old bond and new bonds for the UV(x) excitation (C) and the UV(z) excitation (D). E) and F) FT of the coherence term for the UV(x) and the UV(z) dynamics. The frequencies reflect the oscillation of the two kinds of terms shown in figure 5 of the main text.

4.4 Transient absorption spectra

The linear response transient absorption spectrum[13, 14] is given by $S(\omega) = -2\,\mathrm{Im}\left[\mu(\omega)E^{*}(\omega)\right]$ where $\mu(\omega)$ is the Fourier transform(FT) of the dipole moment $\mu(t)$ computed for the dynamics including the interaction with the pump and the probe pulse and $E(\omega)$ is the complex conjugate of the electric field in the frequency domain generated by the two pulses, both computed for positive frequencies, ω . A positive value of the response function, $S(\omega)$, corresponds to an absorption process, while a negative value corresponds to emission.

The dipole moment $\mu(t)$, also called the total polarization, is given by $\mu(t)=\mathrm{Tr}\left[\hat{\mu}\rho(t)\right]$ where $\rho(t)$ is the coherent density matrix of the system:

$$\mu(t)=\sum_{i,j}\sum_{g}\mu_{ij,g}c_j^*(t)c_i(t)=\sum_{i}\left|c_i(t)\right|^2\mu_{ii,g}+2\,\mathrm{Re}\sum_{i>j}\mu_{ij,g}c_j^*(t)c_i(t) \quad \text{(S19)}$$

where $\mu_{ii,g}$ is the permanent dipole of electronic state *i* and $\mu_{ij,g}$ the transition dipole between the electronic states *i* and *j*. The dipole moments $\mu_{ij,g}$, are observables corresponding to the one electron dipole operator computed at the geometry of the grid point *g*:

$$\mu_{ij,g}=\int d\mathbf{r}\rho_{ij,g}^{elec}(\mathbf{r})\mathbf{r} \quad \text{(S20)}$$

where ***r*** is the electronic coordinate. The dipoles moments are therefore observables of the electronic density and can be used to probe its motion in and out the C-C regions during the ring closure.

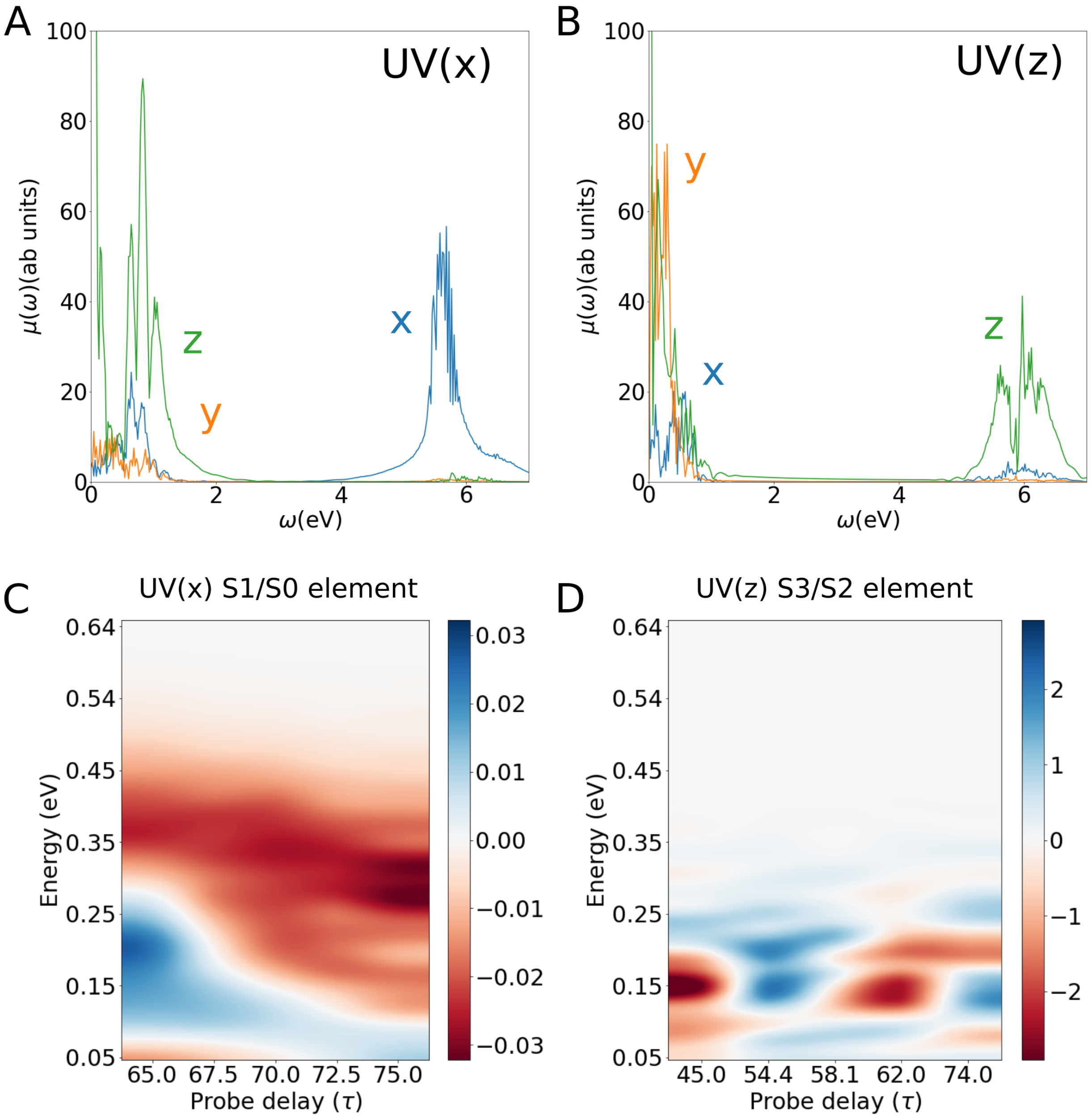

Figure S10: The Fourier transforms of the total dipole moment and transient absorption spectra. Panels A and B: Cartesian components of the total dipole moment, Eq.(S19), computed for the UV(x) dynamics (panel A) and the UV(z) dynamics (panel B). The time dependent components are shown in Figure 6 of the main text. Note the peak at ~6 eV in the x component for the UV(x) dynamics and in the z component for the UV(z) that corresponds to the GS-S$_1$ and GS-S$_2$ transition frequencies in the Franck-Condon region respectively. Note also how the y component, that is used to probe the S$_2$/S$_3$ coherence is more intense in the UV(z) dynamics. The component along z at low frequencies is similar in both dynamics. The higher frequencies at about 0.4-1.5 eV reflect the

S1/S4 electronic coherence while the smaller ones around 0.2 eV reflect the dynamics on S_1 and that at the S_1/S_0 CI. Panel C and D: Transient absorption spectra computed from a single transition dipole term in Eq. (S19) above. C: UV(x) dynamics: only the S_1-S_0 transition dipole term is used in Eq. (S19). D: UV(z) dynamics: only the S_2-S_3 transition dipole term is used in Eq. (S19). Compare with Figure 6 of the main text.

In the case of the UV(x) dynamics, five values of delay times τ have been selected: 65.0, 67.5, 70.0, 72.5 and 75.0 fs. The element corresponding at the S_1/S_0 transition is shown in Figure S10 C. The maximum rate of population transfer occurs at 70 fs. One can see by comparing with Figure 6 of the main text, panel C that the signal at 0.15 eV is essentially due to the S_1/S_0 transition dipole that is beating because of the S_0/S_1 electronic coherence.

In the case of the UV(z) computation, the delay time, τ, spans a whole period: 45.0, 50.8, 54.37, 58.08, 62.00 and 74.00 fs. At 58.1 fs, the wavefunction is localized in regions where the energy difference between S2 and S3 is very low which corresponds to a period of circa 20 fs (0.2 eV). It this case too, the total signal shown in Figure 6 is dominated by the transition S_3/S_2 element shown in Figure S10A and the oscillations of the transient absorption signal at 0.15 eV reflect the oscillations of the S_3/S_2 electronic coherence.

References

1.I. F. Galván, M. Vacher, A. Alavi, C. Angeli, F. Aquilante, J. Autschbach, J. J. Bao, S. I. Bokarev, N. A. Bogdanov, R. K. Carlson, L. F. Chibotaru, J. Creutzberg, N. Dattani, M. G. Delcey, S. S. Dong, A. Dreuw, L. Freitag, L. M. Frutos, L. Gagliardi, F. Gendron, A. Giussani, L. González, G. Grell, M. Guo, C. E. Hoyer, M. Johansson, S. Keller, S. Knecht, G. Kovačević, E. Källman, G. Li Manni, M. Lundberg, Y. Ma, S. Mai, J. P. Malhado, P. Å. Malmqvist, P. Marquetand, S. A. Mewes, J. Norell, M. Olivucci, M. Oppel, Q. M. Phung, K. Pierloot, F. Plasser, M. Reiher, A. M. Sand, I. Schapiro, P. Sharma, C. J. Stein, L. K. Sørensen, D. G. Truhlar, M. Ugandi, L. Ungur, A. Valentini, S. Vancoillie, V. Veryazov, O. Weser, T. A. Wesołowski, P.-O. Widmark, S. Wouters, A. Zech, J. P. Zobel and R. Lindh, *J. Chem. Theory Comput.*, 2019, **15**, 5925-5964.
2.B. O. Roos, M. Merchan, R. McDiarmid and X. Xing, *Journal of the American Chemical Society*, 1994, **116**, 5927-5936.
3.X. Xing, A. Gedanken, A.-H. Sheybani and R. McDiarmid, *J. Phys. Chem.*, 1994, **98**, 8302-8309.
4.W. Fuß, K. K. Pushpa, W. E. Schmid and S. A. Trushin, *Photochemical & Photobiological Sciences*, 2002, **1**, 60-66.
5.I. Antol, *J. Comput. Chem.*, 2013, **34**, 1439-1445.
6.F. Rudakov and P. M. Weber, *J. Chem. Phys.*, 2012, **136**, 134303.

7.I. F. Galván, M. G. Delcey, T. B. Pedersen, F. Aquilante and R. Lindh, *J. Chem. Theory Comput.*, 2016, **12**, 3636-3653.
8.E. Mátyus, G. Czakó and A. G. Császár, *J. Chem. Phys.*, 2009, **130**, 134112.
9.B. Podolsky, *Phys. Rev.*, 1928, **32**, 812-816.
10.S. A. Jayantha, K. G. Komarova, S. v. d. Wildenberg, F. Remacle and R. D. Levine, in *Attosecond Molecular Dynamics*, eds. M. J. J. Vrakking and F. Lepine, Royal Society of Chemistry, Cambridge, 2018, vol. 13, pp. 308-347.
11.K. G. Komarova, F. Remacle and R. D. Levine, *Mol. Phys.*, 2018, **116**, 2524-2532.
12.M. Abramovitz and I. Stegun, *A Handbook of Mathematical Functions*, Dover, New York, 1972.
13.L. Seidner, G. Stock and W. Domcke, *J. Chem. Phys.*, 1995, **103**, 3998-4011.
14.W. Mengxi, C. Shaohao, C. Seth, J. S. Kenneth and B. G. Mette, *J. Phys. B*, 2016, **49**, 062003.